The structure of synchronization sets for noninvertible systems

Krešimir Josić
Department of Mathematics, University of Houston, Houston, Texas 77204

Evelyn Sander
Department of Mathematical Sciences, George Mason University, Fairfax, Virginia 22030

(Received 21 October 2003; accepted 15 January 2004; published online 28 April 2004)

Unidirectionally coupled systems $(x,y)\mapsto(f(x),g(x,y))$ occur naturally, and are used as tractable models of networks with complex interactions. We analyze the structure and bifurcations of attractors in the case the driving system is not invertible, and the response system is dissipative. We discuss both cases in which the driving system is a map, and a strongly dissipative flow. Although this problem was originally motivated by examples of nonlinear synchrony, we show that the ideas presented can be used more generally to study the structure of attractors, and examine interactions between coupled systems. © *2004 American Institute of Physics.* [DOI: 10.1063/1.1667632]

Synchronization in networks of systems with complex behavior has been a topic of extensive experimental and theoretical study in recent years.[1–3] Roughly, a network is synchronized when there is a dynamical relationship among all of its constituent pieces, so that information about any one system can be gained by observing the behavior of another system in the network. More specifically, coupled systems exhibit *generalized synchrony* if the global attractor is contained within a *synchronization set* with an organized structure.[4,5] In many cases, the synchronization set is the graph of a smooth map. However, coupled systems may still be synchronized even when its synchronization set is more complicated. In this paper, we consider the case in which the synchronization set is the graph of multiple curves as a result of noninvertibility of one of the component systems.[6,7,9,14] We provide a mathematical justification of many claims made in our earlier paper.[7] In addition, we extend the work by studying the implications of results obtained for noninvertible maps to flows, analyzing the bifurcations leading to the complicated structures we observe, and explaining how these observations carry over to higher dimensional maps. In this context we also give an explanation of a synchronization detection technique which was recently introduced by He, Zhang, and Stone,[10] and answer an open problem posed by Afraimovich *et al.*[6]

I. INTRODUCTION

A class of models frequently used in the study of synchrony is unidirectionally coupled systems

$$(x,y)\mapsto(f(x),g(x,y)), \tag{1}$$

also known as drive–response, or skew product systems. When the driving map f is invertible and f and g are smooth, it is known that for sufficiently strong coupling the synchronization set is contained in the graph of a smooth function $\phi:X\to Y$ from the drive space X to the response space Y (see Sec. III and Ref. 11 for a precise statement).

In many important cases the driving system $x\mapsto f(x)$ is noninvertible. This can occur if the driving system is obtained by reconstruction and the sampling dimension is too small, if a stroboscopic equation for a differential equation is sampled too infrequently,[12] or as a result of inherent noninvertibility, as in delay equations or numerical approximations.[13] It has recently been observed that in such situations the synchronization set may lose the structure of a smooth manifold, hampering traditional detection methods.[6,7,10,14]

A synchronization set with a structure typical of such examples is shown in Fig. 1, and is discussed in Sec. II. In this case the synchronization set has the structure of the image of a Cantor set of lines in the vicinity of most points. We will show that such structures can be generally expected when the drive is noninvertible, although the local geometry is typically even more complex. Similar structures can be observed in higher dimensional maps, as well as flows which project to noninvertible maps along strong stable foliations. The synchronization set can be multivalued even for invertible maps, although in this case the structure of the synchronization set is very different.[15] We note that the fine structure of the attractors that occurs in phase synchronization has a different origin.[16]

In this paper we discuss the structure and bifurcations of synchronization sets in the presence of noninvertible drives, including representative examples illustrating the types of possible behavior. The paper proceeds as follows: In Sec. II we present a number of examples of multivalued synchronization sets in coupled systems with noninvertible drives and bifurcations that lead to such attractors. In Sec. III, we indicate how to extend the standard proofs which work for invertible systems to show the existence and continuity of synchronization sets in the present case. In Sec. IV, we use a constructive approach to show continuity. This has the advantage of giving more detailed structural information, which is illustrated in several simple examples. The synchronization set may be the union of graphs of uncountable or countable number of continuous functions. We give an example of a synchronization set comprised of a countable number of graphs when the drive has positive topological

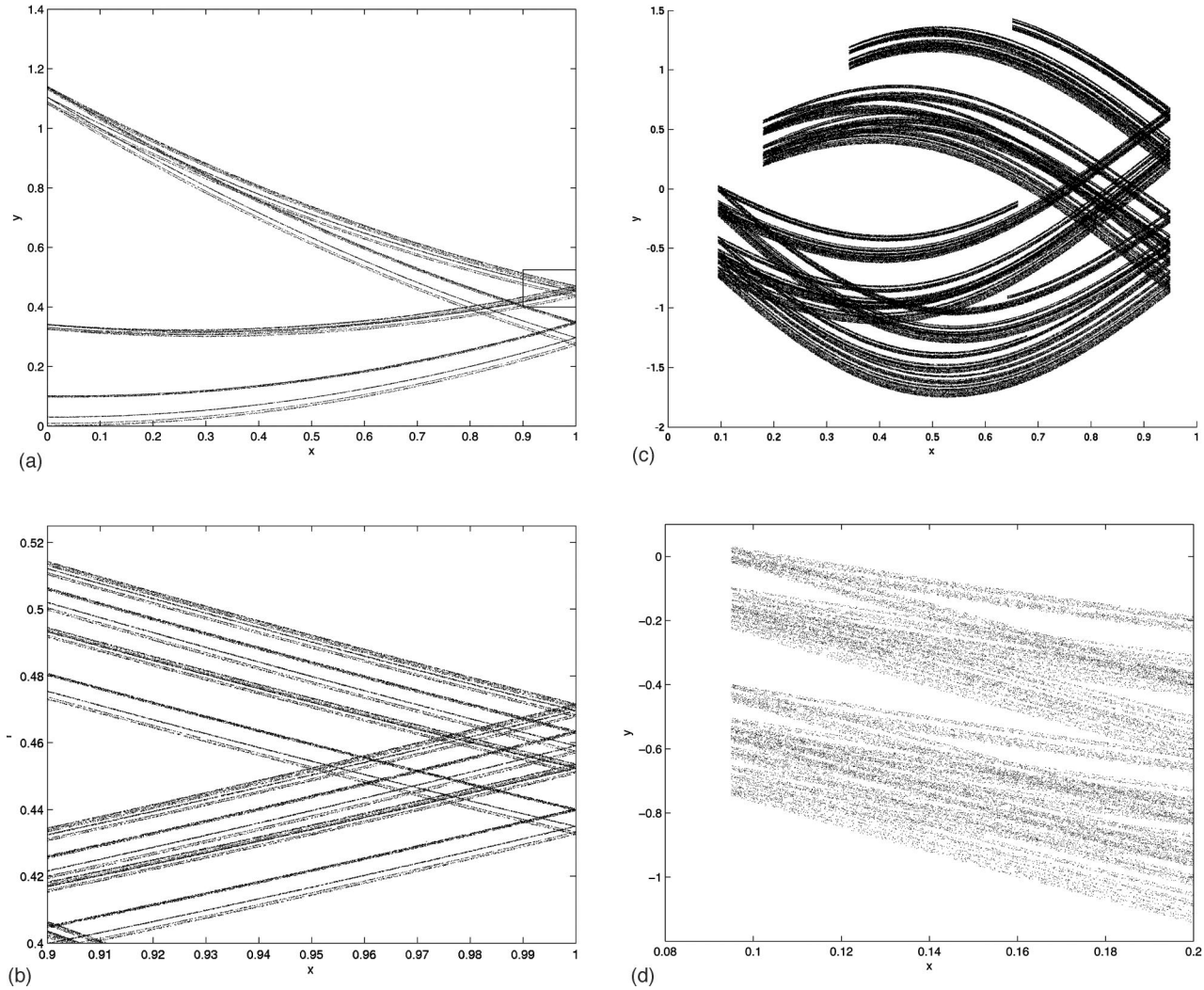

FIG. 1. (a) The synchronization set for a drive–response system in which f is the tent map. (b) A blowup of the square in the a shows the rich Cantor-type structure of the attractor. (c) The synchronization set for a drive–response system in which f is the tent sine map described in the text, and the orbit of the critical point is finite. (d) A blowup of (c).

entropy, answering a question posed in Ref. 6, and show that in pathological cases, the synchronization set can lose the structure of a union of curves. In Secs. IV E and IV F, we use inverse limit techniques to establish the validity of the ϵ-δ^p method for the detection of generalized synchrony for systems with noninvertible driving maps described in Ref. 10. Section V revisits the examples from Sec. II C, giving a proof that typically the synchronization set is nearly smooth and nonintersecting near the bifurcation to a noninvertible drive. In Sec. VI, we give an alternative construction for synchronization sets which can be used to prove smoothness of individual curves within the family.

To avoid introducing cumbersome notation into the examples and arguments, we primarily discuss noninvertible systems in one dimension. Most of the arguments can be extended to higher dimensional systems in a straightforward way.

II. EXAMPLES OF COUPLED SYSTEMS WITH NONINVERTIBLE DRIVES

In this section we consider examples of drive–response system that illustrate the typical phenomena that can be expected in such systems. The general ideas illustrated in these examples will be studied in subsequent sections.

A. Unimodal maps of the interval

The simplest example of noninvertible drive in a system of the form of Eq. (1) is one for which the drive is a tent map

$$f(x)=\begin{cases} cx & \text{if } x\in[0,1/2) \\ -cx+c & \text{if } x\in[1/2,1], \end{cases} \tag{2}$$

where $c\in(0,2]$. As long as the response $g(x,y)$ is contracting in the second variable, the attractor within $[0,1]\times Y$ will be contained in a collection of lines which are connected along the forward orbit of the critical point. If $c=2$ the forward orbit of the critical point is $(\{1/2,1,0,0,\ldots\})$. Since this orbit is finite the vertical line $x=$const. intersects this collection in a Cantor set of points in most places. The different lines in this collection are joined along "hooks" that occur above the forward orbit of the critical point, and may intersect at other points. This situation is illustrated in Figs. 1(a)

and 1(b) with $g(x,y)=dy+x^2$, $d=0.3$, and $c\approx 2$. (See Remark IV.5 for a comment on the numerical implementation.)

The orbit of the critical point is in general not finite for unimodal maps and may be dense in [0,1]. In such situation, the hooks may appear densely throughout the synchronization set. Using visual inspection, the cases of finite and infinite critical orbits appear similar. Figure 1(c) was obtained by using (2) as a drive, with response $g(x,y)=ky+\sin(2\pi x)$, and $c=1.9$ and $k=0.5$. In this case, the orbit of the critical point does not have a low period. The synchronization set appears to be a set of curves; however, the magnification shown in Fig. 1(d) shows that hooks appear throughout the synchronization set, over the forward orbit of the critical point. In the case where the forward orbit of the critical point is dense, under repeated magnification one would see that hooks occur arbitrarily close to any point in the synchronization set. This structure is further explained in Sec. IV.

B. Drives with strong stable foliations

The synchronization set can have a similar structure for strongly dissipative flows. The attractors for such flows frequently possess strong stable foliations along which the dynamics project to lower dimensional noninvertible maps. The Lorenz system in the standard chaotic regime ($\sigma=10,\rho=28.0,\beta=8/3$) has this property. The Poincaré map taken at $z=27$ has an attractor with a strong stable foliation along which the system projects to a noninvertible map of the interval.[17,18] If such a system is used as a drive, the synchronization set can display the structure shown in the previous example.

Consider the Lorenz system $x'=\sigma(y-x), y'=\rho x-y-xz, z'=-\beta z+xy$ driving the system $r'=-cr+x$. The fibers $(x,y,z)=\text{const}$ are contracted under the flow of this system, and the intersection of its attractor with the hyperplane $z=27$ has a local structure that resembles a Cantor set of lines (see Fig. 2). Similar results can be obtained by using any combination of the x and y variable to drive a response system that is uniformly contracting.

As will be shown in Sec. VI, we can think of Fig. 2(b) as a nonlinear magnification of the intersection of the Lorenz attractor with the Poincaré surface $z=27$. Due to the high rate of contraction, the fractal structure of the Lorenz attractor is hard to resolve on the surface $z=27$, and the intersection of the attractor with this section appears as four lines. As shown in Fig. 2, under ''magnification'' these lines are resolved to what appears to be a Cantor set of lines. Lorenz already noted that, although the attractor appears to be a surface due to high dissipation, it has to have a complicated transversal structure.[19] It is this structure that becomes apparent after magnification. These observations are not affected by small noise, and could therefore be useful in studying the attractors of highly dissipative systems from experimental data.

The Rössler attractor also appears to have a similar strong stable foliation, and if used as a drive in $x'=-y-z, y'=x+0.15y, z'=zx-10z+0.2, r'=-cr+x$ with $c=0.2$, we obtain the attractor shown in Fig. 3. As the Poincaré map looks like a ''fattened'' unimodal map, the structure of the attractor in this section appears as a collection of lines joined along the forward orbit of the critical point of this map. Note the similarity between this attractor and that in

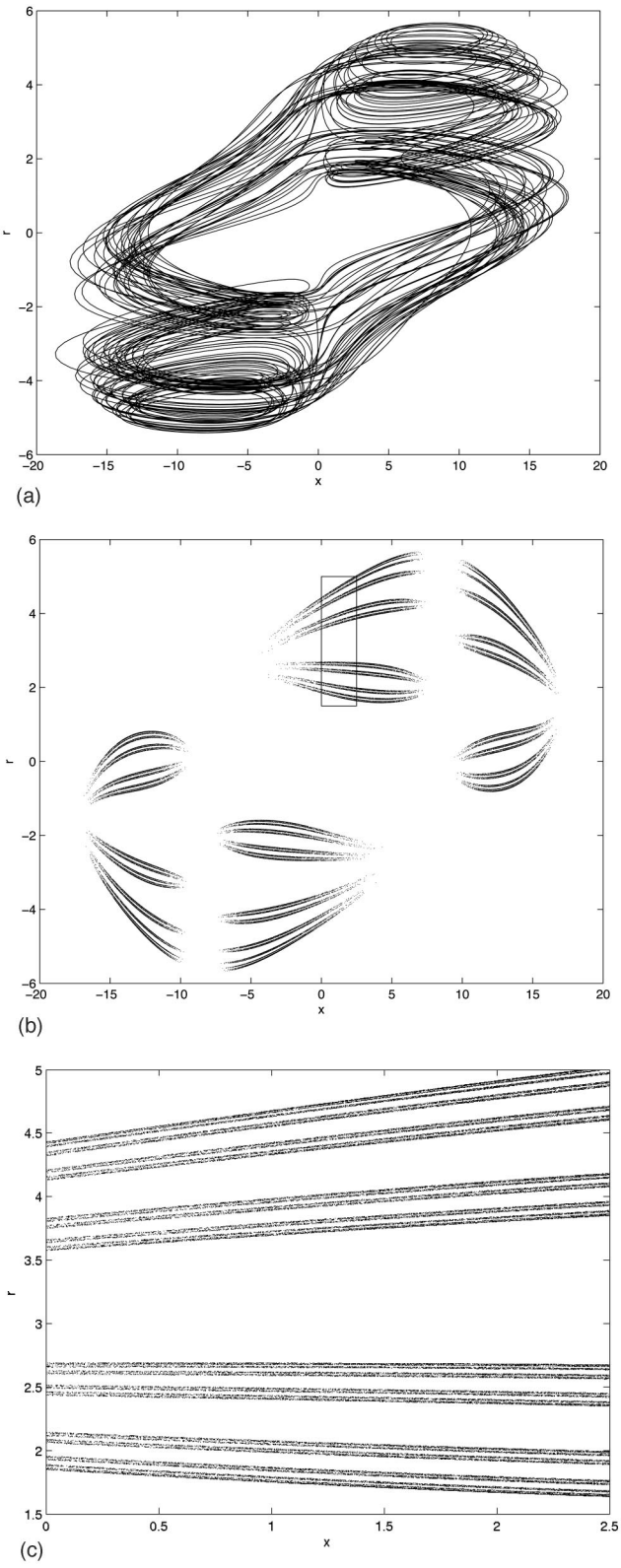

FIG. 2. (a) Lorenz system in the standard chaotic regime ($\sigma=10,\rho=28.0,\beta=8/3$) driving a linear response $r'=-cr+x$. This gives the projection of the attractor from $\mathbb{R}^3\times\mathbb{R}$ onto the x and r variables. (b) The section $z=27$ of the attractor. (c) A blowup of the square in (b) shows the Cantor-type structure in this example.

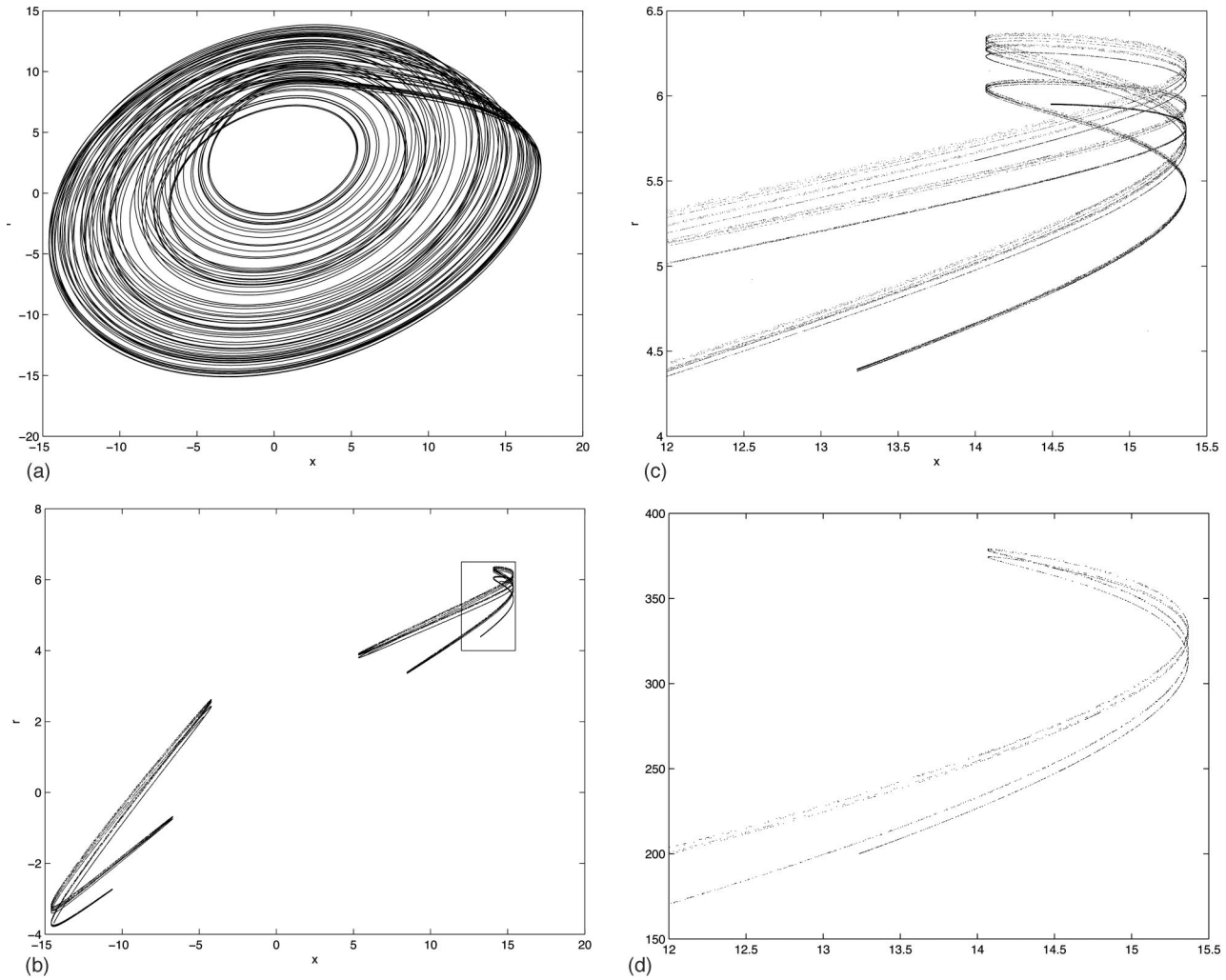

FIG. 3. (a) A projection of attractor of Rössler system used as a drive with response $r' = -cr + x$, $c = 0.2$ from $\mathbb{R}^3 \times \mathbb{R}$ onto the $x-r$ plane. (b) Projection of the section $y = 0$ of the attractor on the left. (c) A blowup of the square in (b) shows the Cantor-type structure in this example. (d) A blowup of the attractor of the same drive and response $r' = -cr + x + y^2$, with $c = 0.2$.

Fig. 1. A comparison of two different response systems is shown in Figs. 3(c) and 3(d). Although the Poincaré section $y = 0$ of the attractors looks different, the hooks still have the same x,z coordinates. Similar results can be expected to hold for other strongly dissipative systems.

C. The onset of noninvertibility

In this section we illustrate the transition from a synchronization set contained in the graph of an interval (as the result of an invertible drive) to one which is contained in the graph of a multivalued function (as the result of a noninvertible drive). Two types of transitions are illustrated in Fig. 4. Also see the URL in Ref. 20 for an animated version of this figure.

Following Ref. 7, we introduce a two-parameter family of drive–response systems

$$u_{n+1} = \begin{cases} \lambda\,\omega(u_n, s, \rho) & v_n < \alpha \\ \lambda + (1-\lambda)u_n & v_n \geqslant \alpha, \end{cases}$$

$$v_{n+1} = \begin{cases} v_n/\alpha & v_n < \alpha \\ (v_n - \alpha)/(1-\alpha) & v_n \geqslant \alpha, \end{cases}$$

$$y_{n+1} = c y_n + \cos(2\pi u_{n+1}), \tag{3}$$

where $(u,v) \in [0,1]\times[0,1]$, $0<\lambda<1$ and $0<\alpha<1$, $1>c\geqslant 0$, while s and ρ are parameters which will be varied. The (u,v) subsystem, which serves as the drive, is a generalized baker's map. The lower portion of the square is mapped by $\omega(u,s,\rho)$, a function of u depending on the parameters s and ρ.

In Ref. 7 a one-parameter family $\omega(u,s,\rho) = \omega(u,s):[0,1]\to[0,1]$ of cubic functions determined by the conditions $\omega(0,s)=0, \omega(1/2,s)=1/2$, $\omega(1,s)=1$, and $(d\omega/du)(1/2,s)=s$ was used to illustrate this bifurcation [see Fig. 5(b)]. For parameter $s>0$, the function is invertible, and the synchronization set is the graph of a smooth function [see Fig. 4(a)]. The attracting set of system (3) is constant in the v direction, and it is therefore sufficient to plot its projection onto the $u-y$ plane. At $s=0$, the function ω has a

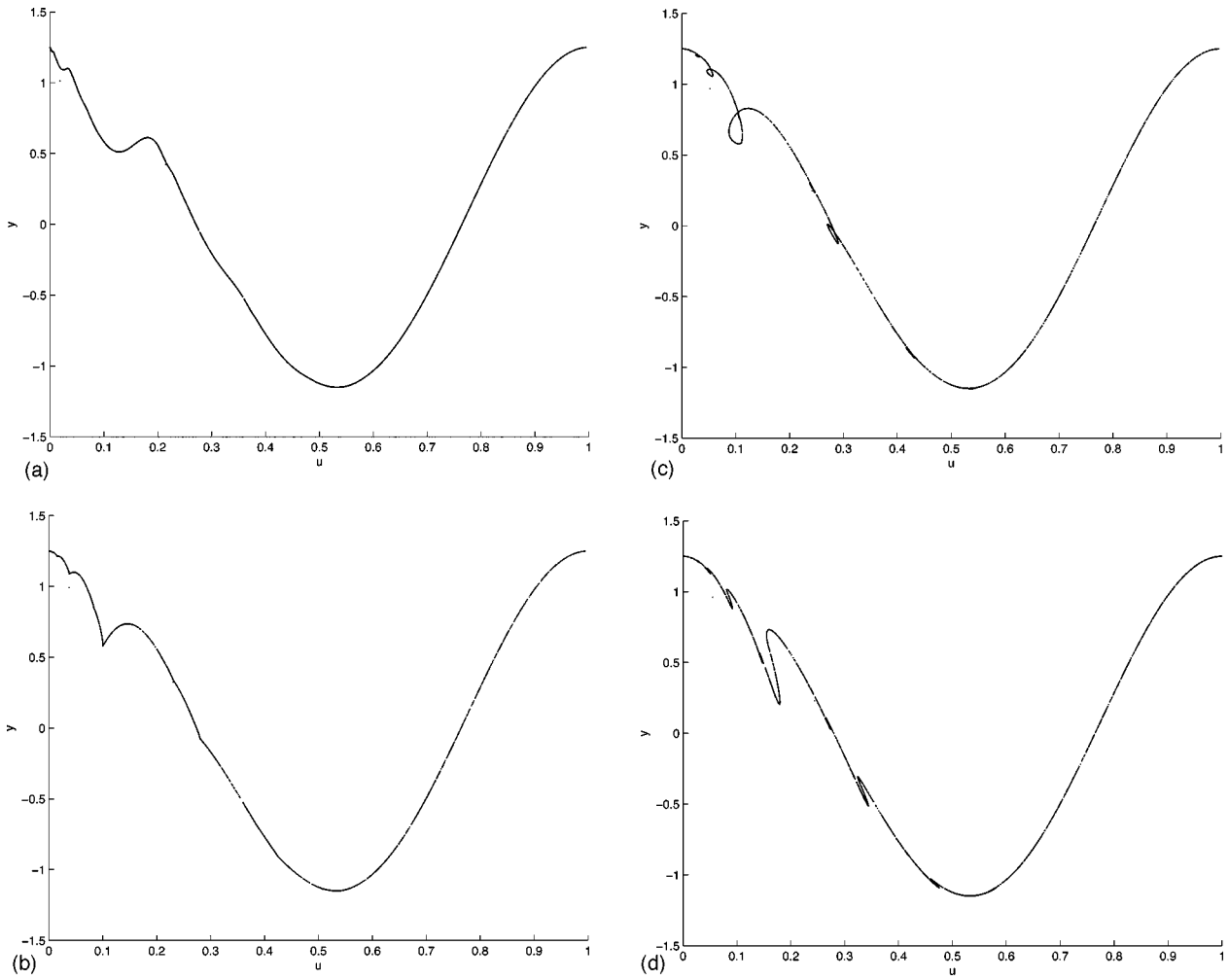

FIG. 4. The attractor of system (3). (a) When the driving map is invertible, the synchronization set is smooth. (b) In special cases, at the onset of noninvertibility the synchronization set appears to develop cusps. (c) As the driving system becomes noninvertible, loops are formed. (d) In a typical transition, places with vertical tangents transition to "bends" in the graph, and no loops appear.

critical point (an inflection point) at $u=1/2$. As a result, cusps seem to develop in the synchronization set, which thereby loses smoothness [see Fig. 4(b)]. When $s<0$, ω_s is noninvertible, the cusps immediately transform to self-intersecting loops [see Fig. 4(c)]. Note that the synchronization set is not a smooth manifold at the bifurcation point $s=0$, and ceases to be a manifold after the bifurcation. In a certain sense, this transition corresponds to a bifurcation of codimension 2, and is therefore atypical.

In Fig. 4(c), notice that at $u\approx 1/2$, the synchronization set has a critical point, the same point at which ω has a critical point. The coincidence of the critical point of the invariant graph and the function ω causes the cusps and the loops.

This simultaneity of the principal critical points is not typical for one-parameter families functions. In the typical case, the invariant graph will transition to a smooth, non-self-intersecting curve, without the appearance of cusps and loops. If there are no cusps, then after the onset of noninvertibility the synchronization set continues to be non-self-intersecting and close to a smooth manifold, although it is no longer the graph of a map. See Fig. 4(d).

To illustrate this, we introduce a parameter ρ, so that the fixed points of $\omega(u,s,\rho)$ are located at 0, ρ, and 1, and such that $(d\omega/du)(\rho,s,\rho)=s$. Changing ρ moves the critical point of ω away from the critical point of the invariant graph (the original map corresponds with the modified function with $\rho=1/2$). As shown in Fig. 5, this results in a transition to a smooth manifold. Cusps occur as a codimension two set in a three-parameter version of this family; specifically, for every c near zero, there is a (s,ρ) pair for which the system has a cusp.

III. AN INVERSE LIMIT APPROACH

We consider the existence of invariant graphs in systems of the form

$$x_{n+1}=f(x_n) \quad f:X\to X,$$
$$y_{n+1}=g(x_n,y_n) \quad g:X\times Y\to Y, \tag{4}$$

where X and Y are smooth, finite-dimensional manifolds possibly with boundary, X is compact, and f and g are continuous but not necessarily invertible. A graph of a function $\phi:X\to Y$ is invariant if $g(x_0,\phi(x_0))=\phi(f(x_0))$, i.e., any point starting on the graph remains on the graph under the evolution of (4).

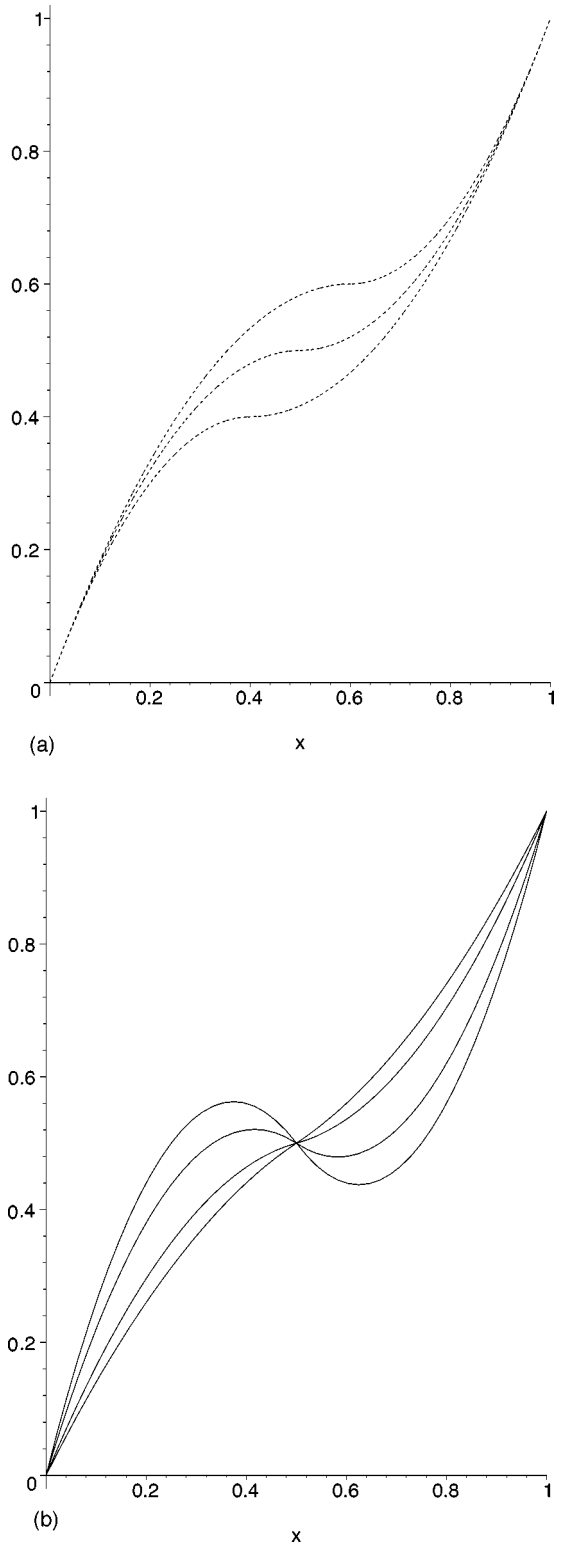

FIG. 5. Graph of $\omega(u,s,\rho)$. (a) Parameter ρ determines the location of the critical fixed point. Values $\rho=0.4,0.5$, and 0.6 are shown. (b) Parameter s determines the slope at the critical fixed point. Values $s=-0.5,0.2$, and 0.5, with $\rho=0.5$ are shown.

The graph transform method, which is typically used in in proving the existence of invariant graphs, relies on the assumption that f is invertible,[21–23] but it can be extended directly to system (4) by considering the inverse limit of X with bonding map f. The inverse limit space (X,f) consists of all sequences $\hat{x}=\{x_0,x_1,x_2,\ldots\}$ such that $f(x_i)=x_{i-1}$ for $i>0$ (cf. Refs. 24, 25 for more details on inverse limits). The map f induces a map $\hat{f}:(X,f)\to(X,f)$ defined by $\hat{f}(x_0,x_1,x_2,\ldots)=(f(x_0),x_0,x_1,\ldots)$. Given an initial sequence $\hat{x}_0$, consider the system

$$\hat{x}_{n+1}=\hat{f}(\hat{x}_n),$$
$$y_{n+1}=g(\pi_0(\hat{x}_n),y_n), \tag{5}$$

where $\pi_0:X\times X\times\cdots\to X$ is the projection onto the first coordinate in the inverse limit space. Note that only the driving systems differ between systems (4) and (5) since the dynamics of the response remains unchanged.

In this context, the graph transform method can be stated as the following theorem:

Theorem III.1 *(Refs. 21,22) Let g and $\hat{f}$ be smooth functions satisfying system (5). For distance metrics d_X and d_Y, assume that there exists a $0<c_1<1$ such that*

$$d_Y(g(\hat{x},y_a),g(\hat{x},y_b))\leqslant c_1 d_Y(y_a,y_b), \tag{6}$$

for all $\hat{x}\in X$ and all $y_a,y_b\in Y$, i.e., the system (4) contracts the fibers $\hat{x}=const$. Assume also that there exists a $c_2>0$ which gives a limit of the contraction in the driving system, i.e.,

$$d_X(\hat{f}^{-1}(\hat{x}_a),\hat{f}^{-1}(\hat{x}_b))\leqslant c_2 d_X(\hat{x}_a,\hat{x}_b), \tag{7}$$

for all $\hat{x}_a,\hat{x}_b\in(X,f)$. Then, there exists a bounded continuous function $\Phi:(X,f)\to Y$ such that the graph of Φ is invariant under $(\hat{f},g)$ and attracting for all $(\hat{x},y)\in(X,f)\times Y$. If $c_1c_2<1$ then this graph is a differentiable manifold.

Variants of this theorem can be proved in cases f or g have less regularity.[26]

IV. THE STRUCTURE OF INVARIANT COLLECTIONS OF GRAPHS

Theorem III.1 implies that, under appropriate conditions, there exists an attracting invariant graph over the inverse limit space of the driving map when the drive is noninvertible. The synchronization set lies in the projection of this graph onto $X\times Y$. The inverse limit space usually has a rather complicated structure,[27,28] which will be inherited by the invariant graph of (4). It is our goal to use a somewhat more direct construction to describe certain features and bifurcations of the attractor of this system. To do this we will define collections of graphs over sequences of intervals, the union of which will equal the projection of the invariant graph in Theorem III.1.

To avoid cumbersome technicalities which would be necessary in the general case, we illustrate how the attractor of system (4) lies in an ''invariant collection of graphs'' in the case where the drive function f is a tent map. Next, we point out how to generalize the construction to Markov maps. A related construction is considered in Ref. 6. In the case of non-Markov maps, an additional step is necessary in the construction, but the essential ideas remain the same. Most ideas presented in this section carry over to dynamics in $\mathbb{R}^{n+1}$.

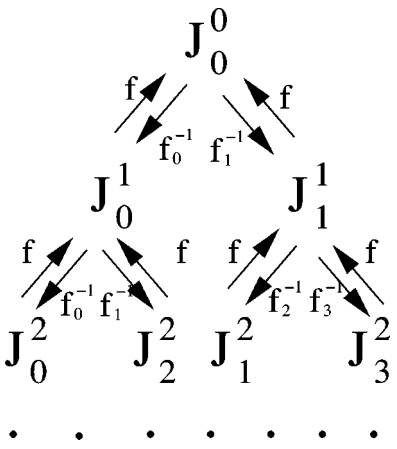

FIG. 6. A tree of intervals for the map (2).

A. Trees and branches

Assume that $g:\mathbb{R}^2\to\mathbb{R}$ satisfies condition (6), and let f be the tent map (2) with $c=2$.

Consider the collection of intervals $J_k^n=[k2^{-n},(k+1)2^{-n}]$ with $0\leqslant k<2^n$. Note that $f(J_k^{n+1})=f(J_{2^n-k}^{n+1})=J_k^n$ and that both maps are invertible when restricted to the intervals $J_{2^n-k}^{n+1}$ and J_k^{n+1}. Therefore, the intervals J_k^n form a tree, so that f maps any interval in the tree to one in the level directly above it, and f is invertible along the branches of the tree. The inverses of f mapping J_k^n to J_k^{n+1} and $J_{2^n-k}^{n+1}$ will be denoted by f_{n+1}^{-1} and $f_{2^n-k}^{-1}$ (see Fig. 6).

Let $a=(a_0,a_1,\ldots)$ be a sequence of integers such that $0\leqslant a_i<2^i$, so that $J_a=(J_{a_0}^0,J_{a_1}^1,J_{a_2}^2,\ldots)$ is a fixed path in this tree, and let

$$G_a=\cup_{a_i}\{\Psi_{a_i}^i|\Psi_{a_i}^i:J_{a_i}^i\to\mathbb{R},\Psi_{a_i}^i\in C(J_{a_i}^i),$$

$$\text{and } \exists B\in\mathbb{R} \text{ such that}|\Psi_{a_i}^i|<B \text{ for all } i\},$$

be the collection of all sequences of bounded, continuous functions, each of which maps an interval in J_a into $\mathbb{R}$. We can define the distance between $\Phi_a,\Psi_a\in G_a$ by

$$\overline{d}_\eta(\Phi_a,\Psi_a)=\sum_{i=0}^{\infty}\frac{d_i(\Phi_{a_i}^i,\Psi_{a_i}^i)}{e^{\eta i}},$$

where $\eta>0$, and d_i is the metric induced by the supremum norm in $C(J_{a_i}^i)$.

Definition IV.1 *The sequence Ψ_a is invariant under (4) if the graph of $\Psi_{a_{i+1}}^{i+1}$ is mapped onto the graph of $\Psi_{a_i}^i$ for $i=0,1,\ldots$. More precisely*

$$\Psi_{a_i}^i(f(x))=g(x,\Psi_{a_{i+1}}^{i+1}(x)), \tag{8}$$

for all x on which $\Psi_{a_{i+1}}^{i+1}$ is defined.

Finally, let S be the set of all integer sequences $a=(a_0,a_1,\ldots)$ with $0\leqslant a_i<2^i$, and let $G=\cup_{a\in S}G_a$, the collections of graphs over the intervals in the entire tree. An element $\Psi\in G$ is a collection of graphs over each possible path in the tree of intervals. Thus, we have three levels at which we can view the collection of maps defined on the tree of intervals: the individual maps $\Psi_{a_i}^i$, sequences of maps Ψ_a, and collections of sequences Ψ.

B. The synchronization set

In this section, we illustrate the proof of the following:

Theorem IV.2 *For a system of the form (4), where f is a continuous piecewise monotone map of the interval with all critical points having finite forward orbits, and g satisfies condition (6), the synchronization set is contained in a collection of continuous graphs.*

Since f is a Markov map, there exists a tree structure analogous to the one described in the previous section, and the synchronization set is a collection of continuous graphs over the intervals that occur as branches in the tree. This sequence is obtained as an invariant element in G.

The proof is a straightforward generalization of the graph transform method to graphs defined over sequences of intervals. We first assume that f is a tent map, and then show that a similar argument works in the general case. The statement is proved by defining a map $\Gamma_a:G_a\to G_a$ which is a contraction, and whose fixed point is the desired graph.

The graph transform is defined as

$$\Gamma_{a_i}(\Psi_{a_i}^i)(x)=g(f_{a_{i+1}}(x),\Psi_{a_{i+1}}^{i+1}(f_{a_{i+1}}^{-1}(x))).$$

Following the construction above, the map $\Gamma_a=(\Gamma_{a_0},\Gamma_{a_1},\ldots)$ is defined to act on sequences of graphs. It is straightforward to check that a fixed point of the map Γ_a satisfies (8), and maps G_a into itself. It remains to check that the map is a contraction, to show the existence of a fixed point Ψ_a^*. This is done in the Appendix.

The argument is independent of the sequence a chosen in the construction. Therefore, the union of all invariant graphs $\cup_{a\in S}\Psi_a^*$ forms an invariant collection of graphs Ψ^*. Under the dynamics of the system, graphs over one level in the tree get mapped to graphs at the next level. Each sequence Ψ_a^* terminates in the top level graph $\Psi_{a_0}^{0*}$. To see where the top level graph is mapped to, note that it is a union of two graphs $\Psi_{b_1}^{1*}$ and $\Psi_{c_1}^{1*}$, where the sequences b and c are defined by $b=(b_0,b_1,b_2,\ldots)=(0,0,a_1,a_2,\ldots)$ and $c=(c_0,c_1,c_2,\ldots)=(0,1,a_1,a_2,\ldots)$, so that the image of $\Psi_{a_0}^{0*}$ must be $\Psi_{b_0}^{0*}\cup\Psi_{c_0}^{0*}$.

By the same argument, the collection of all 2^k graphs that share the same terminating sequence a, but have different initial sequences, i.e., all graphs corresponding to sequences of the form

$$(0,\underbrace{\ldots,\ldots}_{k \text{ fixed symbols}},a_1,a_2,\ldots),$$

the graph corresponding to the sequence $a=(0,a_1,a_2,\ldots)$.

This argument can be used directly to explain the structure of the synchronization set in Figs. 1(a) and 1(b) where f is given by (2) map and $g(x,y)=dy+x^2$. The attractor is contained in a collection of graphs from $[0,1]$ to $\mathbb{R}$. Each of the graphs in this collection is mapped to two graphs connected at $x=1$. Figure 7 illustrates this by showing the first three iterates of the unit square.

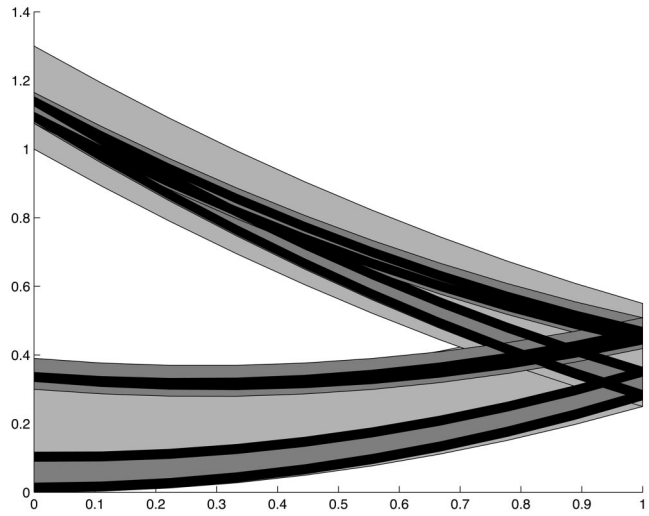

FIG. 7. The light gray, dark gray, and black regions represent, respectively, the first, second, and third iterates of the unit square under the evolution of the drive–response system described in the text [compare with Figs. 1(a) and 1(b)].

The attractor of system (4) is contained in the collection of graphs Ψ, although it is typically only a proper subset.

If f is a piecewise monotone map on $[0,1]$ and the forward orbits of the critical points of f are finite (f is a Markov map), then these orbits provide a finite partition of the interval I into intervals I_k. The preimage of each I_k consists of a union of preimages, each of which lies in a distinct subinterval I_j. We can therefore create k trees of intervals with $I_k = I_k^0$ placed at the root of each tree. The remainder of the tree is constructed exactly as in the case of the tent map discussed above. Repeating the argument outlined above, we can again obtain an invariant collection of graphs. The dynamics of this collection is again determined completely by the path in the tree chosen to construct the graph (which is exactly a symbolic sequence for the Markov map), and the attractor is again contained in this invariant collection (see Ref. 6 for an alternative construction).

Remark IV.3 *This argument only shows that there exists an invariant collection of continuous graphs. The contraction mapping theorems used to prove the smoothness of the invariant manifold in the case of invertible maps are more technical,[21–23] but can be extended to the present case. The smoothness of the invariant manifold can be guaranteed only if the rate of contraction of g given by c_1 in (6) does not exceed the reciprocal of the minimum rate of contraction of f^{-1} given by $1/c_2$ in (7). In the case when f is an expanding map, this condition is always satisfied. However, if f is smooth and noninvertible, then near the singular points $1/c_2$ is unbounded. Orbits that return often to a neighborhood of the these points will also be highly contractive, and the conditions for smoothness may not be satisfied, regardless of the contraction rate c_1 in (6). Estimating the size of the set of orbits on which such high contraction occurs is a delicate question. For a more detailed discussion, see Refs. 7, 9, 23, and 29.*

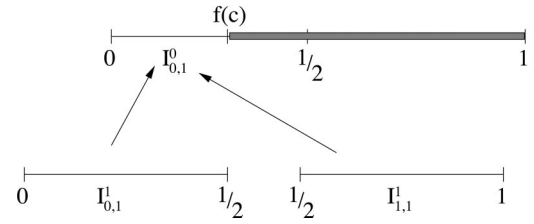

FIG. 8. Constructing the first level of the tree for (2), with $c<1$. The shaded parts of the interval are trimmed at this level.

C. Extensions of the construction

If the orbit of the critical point is not finite, the construction becomes somewhat more involved. In this case only part of an interval that occurs in the construction of the tree may be in the range of f. When this occurs we need to "trim" away the part of the interval that is not in the range. We present two particular examples. Although the first example is trivial, it is chosen to clearly illustrate the general procedure.

Let us again consider the tent map (2), and let $c<1$. Note that in this case f is not an expanding map. We again start the construction of the tree by considering the root interval $I_0^0=[0,1]$. However, the image of the intervals $I_0^1 = [0,1/2]$ and $I_1^1=[1/2,1]$ is $f(I_0^1)=f(I_1^1)=[0,f(c)]$ is not the entire interval. We therefore replace the interval $I_0^0 = [0,1]$ with the interval $[0,f(c)]$ at this level of the construction and obtain two paths $(I_{0,1}^0, I_{0,1}^1)$ and $(I_{0,1}^0, I_{1,1}^1)$, where the second subscript denotes the level of construction (see Fig. 8).

To construct the next level of intervals, note that the interval $I_1^1=[1/2,1]$ has no preimage under f, so the path $(I_{0,1}^0, I_{1,1}^1)$ terminates at this point. On the other hand, the path $(I_{0,1}^0, I_{0,1}^1)$ can be extended to create the next level of paths $(I_{0,2}^0, I_{0,2}^1, I_{0,2}^2)$ and $(I_{0,2}^0, I_{0,2}^1, I_{1,2}^2)$ where $I_{0,2}^0 = [0,f(f(c))], I_{0,2}^1=[0,f(c)], I_{0,2}^2=[0,1/2]$, and $I_{1,2}^2=[1/2,1]$ (see Fig. 9).

This construction can be continued indefinitely, and results in a single path

$$(I_{0,\infty}^0, I_{0,\infty}^1, \ldots, I_{0,\infty}^n, \ldots),$$

with $I_{0,\infty}^n=0$ for all n. Although this is a very indirect way to reach the conclusion that we can only construct an invariant graph over the fixed point $x=0$, it illustrates the generally applicable procedure of trimming intervals along the branches tree.

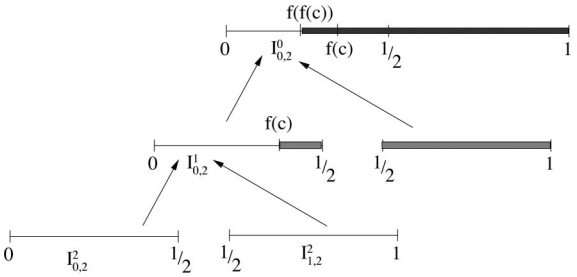

FIG. 9. The second level of the tree for (2), with $c<1$ with shaded parts being trimmed.

The synchronization set in this case only contains one point with x-coordinate 0, and y coordinate determined by the response map. The same construction for the tent map when $c>1$ results in a number of sequences. Some of these sequences may terminate, and some may result in sequences of points rather than intervals. However, in the case of piecewise monotone maps, at least some of the sequences will consist of nondegenerate intervals.[30] Therefore, at least a portion of the synchronization set will consist of graphs of continuous curves over intervals. Unlike the case of Markov maps, in general the topology of the invariant collection of intervals is difficult to determine using this construction. Despite this, we will show in Sec. IV E that we can still approximate the invariant graph with a collection of intervals.

This construction is closely related to the inverse limit construction discussed in Sec. III. The collection of graphs constructed using this procedure corresponds to

$$\bigcup_{x\in(X,f)}(x_0,\Phi(x))=\bigcup_{x\in(X,f),i\in\mathbb{N}}(x_i,\Phi(x)),$$

where $x=\{x_0,x_1,x_2,\dots\}$ is the inverse limit sequence described in Sec. IV E, and $\Phi:(X,f)\to Y$ is the invariant graph over the inverse limit discussed in the previous section. This explains our earlier claim that this graph may be viewed as the projection of the graph Φ onto the first coordinate in the inverse limit. We may also use this observation to conclude that, since the graph Φ is bounded, there exists a C such that $|\Psi^{j}_{a_j,\infty}(x)|<C$ for any graph in the invariant collection.

Remark IV.4 *There are several constructions of inverse limits which are pseudoarcs and therefore do not contain any intervals.[28,31] If the bonding maps used to construct these inverse limits are used in our construction, all sequences of intervals will be degenerate, i.e., all will be sequences of points. Therefore, no points of the synchronization set are contained in continuous curves. As noted, this does not happen for piecewise monotone maps.*

D. Connections between graphs in the invariant collections

It is apparent in Fig. 1(a) that the different graphs in the invariant collection are connected along the forward orbit of the critical point. In this section we show that this is true in the case of a tent map with $c=2$, and discuss how to extend these observations.

In the construction of the tree of intervals in Sec. IV A, each pair of adjacent intervals shares an endpoint. Consider the sequences $\{k_n(1/2)^n\}_{n=0}^{\infty}$, where $k_0=1$ and $f(k_{n+1}(1/2)^{n+1})=k_n(1/2)^n$. Each such sequence corresponds to one possible backward orbit of the critical point 1/2. There are two intervals $J^n_{i_1}$ and $J^n_{i_2}$ which share $k_n(1/2)^n$ as an endpoint. Therefore, there are two paths of intervals, in the tree, such that at each level the two corresponding intervals share an endpoint. Since $k_n(1/2)^n\neq 1/2$, it follows that f is invertible along this path, except at the top level. Therefore, we can take the union of the two intervals at each level to show that our construction gives a unique graph over the interval $[0,1]$ at the first level of the tree. This interval is then mapped to two intervals at the zeroth level of the tree which are joined at the image of the critical point, $f(1/2)=1$.

In Sec. IV A it was shown that the invariant collection of graphs Ψ^* equals the union of top level graphs $\Psi^*_{a_0}$. The argument in the previous paragraph shows that all connections among the top level graphs occur at the critical point and its images. Moreover, two graphs $\Psi^*_{a_0}$ and $\Psi^*_{b_0}$ will be connected if all pairs of intervals $J^k_{a_k}$ and $J^k_{b_k}$ share a common endpoint corresponding to an orbit that eventually lands at a critical point.

The same observation is true more generally. In the extended construction described in Sec. IV C, the intervals in two branches in the extended tree will share a point, if and only if each pair of intervals at a certain level shares an endpoint which eventually maps to a critical point of the map.

As a simple example, consider the map

$$f(x)=\begin{cases}2x & \text{if } x\in\left[0,\dfrac{1}{2}\right),\\ -x+\dfrac{3}{2} & \text{if } x\in\left[\dfrac{1}{2},1\right].\end{cases}\tag{9}$$

The tree of intervals corresponding to this equation has $k+2$ intervals at the kth level, and hence there are only a countable number of branches. Using the argument outlined above, it is immediate that the different branches correspond to intervals that are joint alternately at $x=1/2$ and $x=1$. Not surprisingly, the inverse limit for this map is equivalent to the topologist's sine curve.

A question posed in Ref. 6 is whether the invariant graph can consist of a countably infinite number of curves when the driving map has positive topological entropy. The following example answers the question in the affirmative. It is a drive–response system of the form (4), where the drive is the logistic map $f(x)=\mu_1 x(1-x)$ for $\mu_1=4$. It is well known that this drive has positive topological entropy. The response is given by the formula

$$g(x,y)=h(x)\ \ \mu_2\ \ x(1-x)+(1-h(x))\ \ f(x),\tag{10}$$

and μ_2 chosen to be near 4 (for example, we use $c=3.7$), and h is a differentiable function defined by

$$h(x)=\begin{cases}N(x_1-x)^2 & \text{if } x\in[0,x_1),\\ 0 & \text{if } x\in[x_1,x_2],\\ N(x-x_2)^2 & \text{if } x>x_2,\end{cases}\tag{11}$$

where $x_1=(1-1/\sqrt{2})/2$, $x_1=(1+1/\sqrt{2})/2$, and $N=1/(2x_1^2)$. Note that $f^{-1}([1/2,1])=[x_1,x_2]$. Thus, for $x\in[x_1,x_2]$, $g(x,y)=f(x)$. Thus, the synchronization set is the graph of a single curve for all $x\in[1/2,1]$. This single curve corresponds to many different sequences in the inverse limit space. As a result, the synchronization set consists of a countably rather than uncountably infinite number of curves above the interval $[0,1/2]$. To see this, consider two points $\{x_0,x_1,\dots\}$ and $\{z_0,z_1,\dots\}$ in the inverse limit space for (X,f). If $x_0=z_0>1/2$, then the points correspond to the same point on the synchronization set independent of all other values in the sequence. Therefore, except for a se-

quence with all points less than 1/2, all other points on the synchronization set S are determined by a finite sequence.

The number of curves above the interval (0,1/2) is countably infinite rather than finite. (The curves all intersect at 0 and 1/2.) To show this, we calculate the unique curve Γ_R of S which is a graph over the interval (1/2,1] and the unique curve Γ_0 which is a graph over $[0,1/2]$ with a kth backward orbit in $[0,x_1^{-k}]$ for all k. We use the invariance of the synchronization set; the image of Γ_R under the system has a portion which is a graph over (0,1/2). This is distinct from Γ_0. As a result of this and the fact that f is one-to-one on this interval, every image of these two curves, restricted to (0,1/2), is a distinct curve as well. This gives a countably infinite number of distinct curves.

The previous example is carefully constructed so that many curves in the inverse limit space project onto the same curve in the original space. We conjecture that this nongeneric collapse is necessary in order to have a countable number of curves when the topological entropy is positive.

E. Approximations of the invariant collection

In this section we show that the full invariant collection of graphs can be approximated to arbitrary accuracy by a specific finite collection of graphs when f is uniformly expanding. Therefore, even in very complex situations, the synchronization set looks like a union of curves. The argument is again presented for the case of a tent map (2) with $c=2$, and can be generalized.

For an arbitrary $\epsilon>0$, we will construct a finite set of graphs, each of which will lie within a distance ϵ of an uncountable number of graphs in the invariant collection. The union of these representative graphs provides the desired approximation.

Since f is uniformly expanding, the intervals $J^n_{a_n,n}$ at the nth level of construction in the paths $(J^0_{a_0,n},J^1_{a_1,n},\ldots,J^n_{a_n,n},\ldots)$ have length smaller than $(1/2)^n$, and there exists an N such that $(1/2)^N<\epsilon$. Fix the finite sequence $\{a_0,\ldots,a_N\}$. In the case of the tent map with $c=2$, this first step is not necessary; however, it becomes essential when the orbit of the critical point is not finite.

As noted earlier, all graphs in the invariant collection are bounded by some $C>0$. Let M be such that $Cc_1^M<\epsilon$ where c_1 is defined in (6). Select a fixed sequence $\{a_0,\ldots,a_N,\ldots,a_{N+M}\}$ and continue the construction that was terminated at the level N to the level $N+M$, to obtain the paths $(J^0_{a_0,N+M}\ldots,J^N_{a_N,N+M},\ldots,J^{N+M}_{a_{N+M},N+M})$. Consider the functions $\tilde{\Psi}^{N+M}_{a_{N+M},N+M}=0$ defined over each interval at this level, and consider the Mth forward image of graph $(\tilde{\Psi}^{N+M}_{a_{N+M},N+M})$. This is the graph of a function $\tilde{\Psi}^N_{a_N,N}:I^N_{a_N,N+M}\to Y$. By construction

$$\sup_{x\in I^N_{a_N,\infty}} |\tilde{\Psi}^N_{a_N,N}(x)-\Psi^{N*}_b(x)|<Cc_1^M<\epsilon,$$

where $\Psi^{N,*}_b$ is the Nth graph of *any* sequence Ψ^*_b in the invariant collection such that $\{b_0,\ldots,b_{N+M}\}=\{a_0,\ldots,a_{N+M}\}$, where $\{a_0,\ldots,a_{N+M}\}$ is the sequence fixed in the previous step. Therefore, $\tilde{\Psi}^N_{a_N,N}(x)$ gives an ϵ approximation of any graph in the invariant collection corresponding to a sequence that starts with $\{a_0,\ldots,a_{N+M}\}$. Taking the finite union of graphs corresponding to all possible starting segments $\{a_0,\ldots,a_{N+M}\}$ gives an ϵ approximation of the entire invariant collection.

This argument can be extended to the case of nonuniformly expanding maps, and maps that are expanding on average by modifying the choice of μ. Therefore, regardless of the topological complexity of the invariant collection, it can always be approximated by nearly invariant collection consisting of finitely many graphs.

Remark IV.5 *In Figs. 1(a) and 1(b), we took* $c=1.9999$, *since binary arithmetic makes numerical analysis of the case* $c=2$ *difficult. The results of this section show that the invariant collections of graphs in the two cases will be close. This follows from the facts that only a finite number of images are necessary to construct an arbitrarily good approximation of the collection, and the dynamics depends continuously (even differentiably) on the parameter* c.

F. A note on detection methods

In Ref. 9 it was shown that methods that rely on continuity for the detection of synchronous states typically fail in the case of noninvertible systems. A typical example is given by the ϵ-δ method, where one chooses a ball $B(x,\delta)$ around a reference point x, and iterates the driving system in (4) until the orbit falls within $B(x,\delta)$ a large number of times. To each point $x_{a_i}\in B(x,\delta)$ on the orbit, there corresponds a point $y_{a_i}\in Y$ such that (x_{a_i},y_{a_i}) lies on the attractor of (4). Let ϵ be the radius of the smallest ball in y containing all y_{a_i}. If the attractor lies in a smooth or Lipschitz manifold, then ϵ decreases linearly with δ. If f is noninvertible, the attractor will be in a collection of graphs. In this case ϵ will typically not decay with δ because nearby points in $B(x,\delta)$ may have different histories, and the corresponding points y_i may not lie on the same graph.

In Ref. 10 it was argued that a modification of the method can be applied to detect synchronization in the case where f is noninvertible. Let x^* and z^* be two points on the orbit of x_0 and z_0 on the attractor, under the evolution of the driving system. Consider the subsets of the orbits of x_0 and z_0 defined by $\mathbf{x}^*_p=(x_n,f(x_n),\ldots,f^{p-1}(x_n))$, where x_n is some point on the orbit of x_0 satisfying $f^{p-1}(x_n)=x^*$, and $\mathbf{z}^*_p=(z_m,f(z_m),\ldots,f^{p-1}(z_m)=z^*)$ (note that m does not have to equal n). The point z^* is said to be δ^p close to x^* if $|f^k(x_n)-f^k(z_m)|<\delta$ for all $0<k<p-1$, so that entire portions of the orbits of x_0 and z_0 consisting of p points are required to be δ close. This notion of distance and the associated ϵ-δ^p test can be used to detect synchrony even when f is noninvertible.

The effectiveness of this method can be explained using the ideas described in the previous section. We again consider the tent map (2) with $c=2$ as an illustrative case. Two points x^* and z^* are δ^p close, if their partial orbits $x^*_p=(x_n,f(x_n),\ldots,f^{p-1}(x_n)=x^*)$ and $\mathbf{z}^*_p=(z_m,f(z_m),\ldots,f^{p-1}(z_m)=z^*)$ constitute the head of two close-by elements of the inverse limit space. This means that

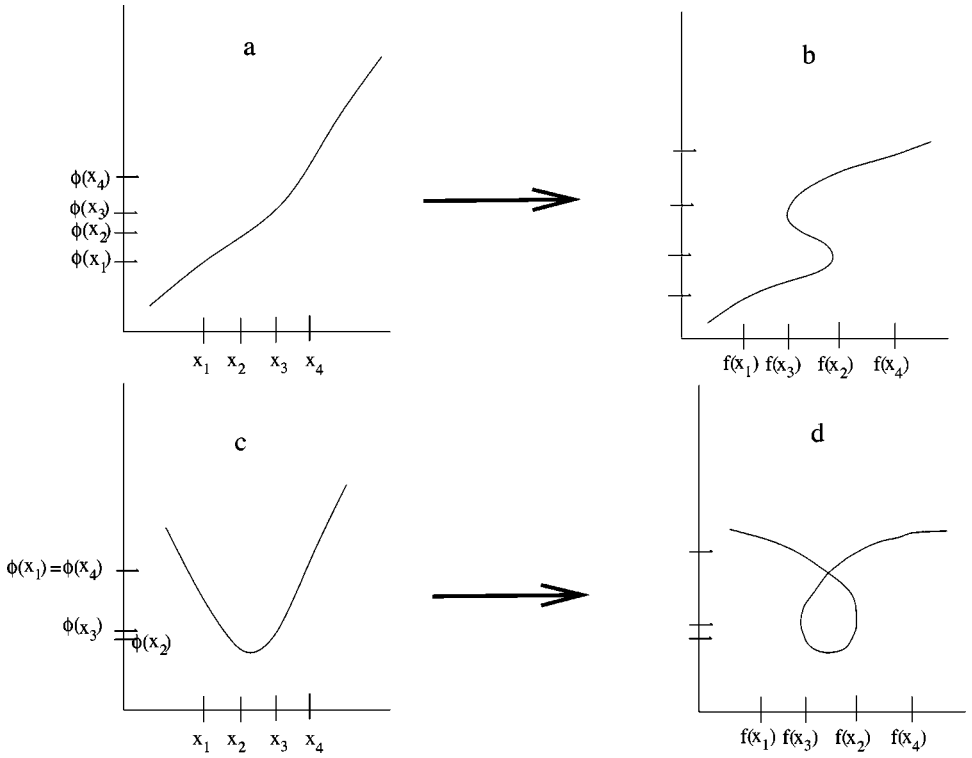

FIG. 10. (a) When ϕ is a monotone graph of a function near x, then (b) the synchronization set near $f(x)$ becomes multivalued without containing self-intersections. (c) If the synchronization set has a critical point corresponding to a critical point x of f, then (d) the synchronization set contains point of self-intersection, or loops, immediately upon becoming multivalued.

most likely $f^k(z_m), f^k(x_n) \in J_a^{p-k-1}$ for some sequence a and intervals $J_a^0,\ldots,J_a^{p-1}$ in the tree defined in Sec. IV A. Since only the head of the two symbolic sequences corresponding to x^* and z^* is required to match, their images do not necessarily lie on the same graph. However, we know that the points $\Psi_a^0(x^*)$ and $\Psi_b^0(z^*)$ in the invariant collection correspond to two sequences a and b such that $\{a_0,\ldots,a_{p-1}\} = \{b_0,\ldots,b_{p-1}\}$. Therefore

$$
\begin{aligned}
&|\Psi_a^0(x^*)-\Psi_b^0(z^*)| \\
&\quad \leqslant (|\Psi_a^0(x^*)-\Psi_a^0(z^*)|+|\Psi_a^0(z^*)-\Psi_b^0(z^*)|) \\
&\quad \leqslant \epsilon(\delta,x^*)+c_2^{p-1}|\Psi_a^{p-1}(z_m)-\Psi_b^{p-1}(z_m)| \\
&\quad \leqslant \epsilon(\delta,x^*)+c_2^{p-1}C, \qquad (12)
\end{aligned}
$$

where c_2 is defined in (6), C is the size of the attractor in the vertical direction, and $\epsilon(\delta,x^*)=\max_{z\in B(x^*,\delta)\cap J_a^0}|\Psi_a^0(z) -\Psi_a^0(x^*)|$. As in the invertible case, $\epsilon(\delta,x^*)$ will decay to 0, and it will decay linearly if $\Psi^0-a(x^*)$ is differentiable or Lipschitz at x^*.

Therefore, if the attractor of the system is contained in an invariant collection of continuous graphs, the ϵ-δ^p method can be used to analyze the regularity of the graphs in this collection. Increasing p decreases $c_2^{p-1}C$, and therefore the resolution of the method.

V. BIFURCATION TO A NONINVERTIBLE DRIVE

An example in Sec. II C illustrated how the invariant graph either developed hooks [Fig. 10(b)], or loops [Fig. 10(d)] as the map defining the driving system changes from being invertible to noninvertible. In this section we provide a heuristic argument why typically near the bifurcation, the invariant graph is close to a smooth manifold without self-intersecting loops.

Consider a system $(x,y)\mapsto(f(x),g(f(x),y))$ with $y \in \mathbb{R}$. The idea of the argument is illustrated in Fig. 10. Assume that we have a piece of a graph $\phi(x)$. Choose four points $x_1<x_2<x_3<x_4$ in the domain of the graph. We assume that the response system contracts the y direction, and that ϕ does not change the ordering of the points, so that $\phi(x_1)<\phi(x_2)<\phi(x_3)<\phi(x_4)$. Also assume that $f:\mathbb{R}\to\mathbb{R}$ has the shape of the cubic with two critical points at x_2 and x_3 [see Fig. 5(b)], so that $f(x_1)<f(x_3)<f(x_2)<f(x_4)$. If ϕ is monotone between x_1 and x_4 [as in Fig. 10(a)], it is easy to see that the image of the graph of ϕ will be nonintersecting [as in Fig. 10(b)]. On the other hand, if ϕ has a critical point between x_2 and x_3 [see Fig. 10(c)], a loop will be formed under one iterate [shown in Fig. 10(d)].

More formally, the synchronization set is contained in the invariant graph of a function ϕ which satisfies $\phi(f(x)) = g(f(x),\phi(x))$. Assume that the f is a monotone increasing function such that $f'(x_*)=0$ [see the middle graph in Fig. 5(a)]. Then, $f'(x)$ has the same sign for all $x\neq x_*$. The tangent of S is such that

$$
\begin{aligned}
\phi'(f(x))f'(x) &= D_1 g(f(x),\phi(x))f'(x) \\
&\quad + D_2 g(f(x),\phi(x))\phi'(x),
\end{aligned}
$$

whenever $\phi'(x_*)D_2g(f(x_*),\phi(x_*))\neq 0$, $\phi'(f(x_*))$ limits to a well-defined vertical tangent ∞ or $-\infty$, corresponding to the sign of $f'(x)$ for $x\neq x_*$. Therefore, by the implicit function theorem, the synchronization set can be written as the graph of a smooth function $x=\eta(y)$ from Y to X. For nearby parameter values, this smoothness may not persist, as

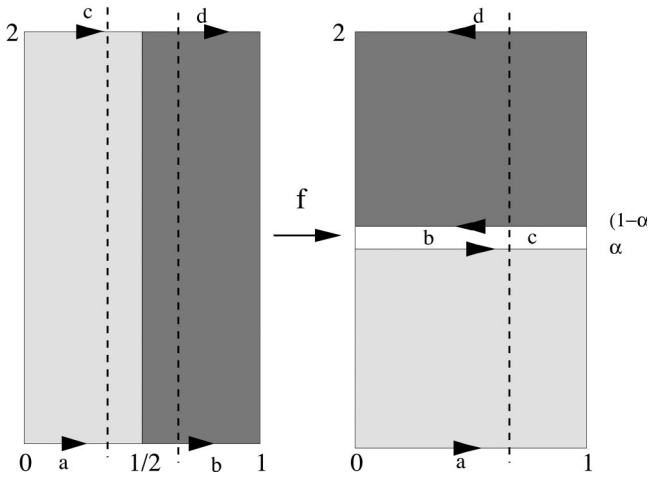

FIG. 11. A schematic of baker's map which can be thought of as an extension of the tent map. The two dotted lines on the left are preimages of the dotted line on the right, and project to a point under ϕ.

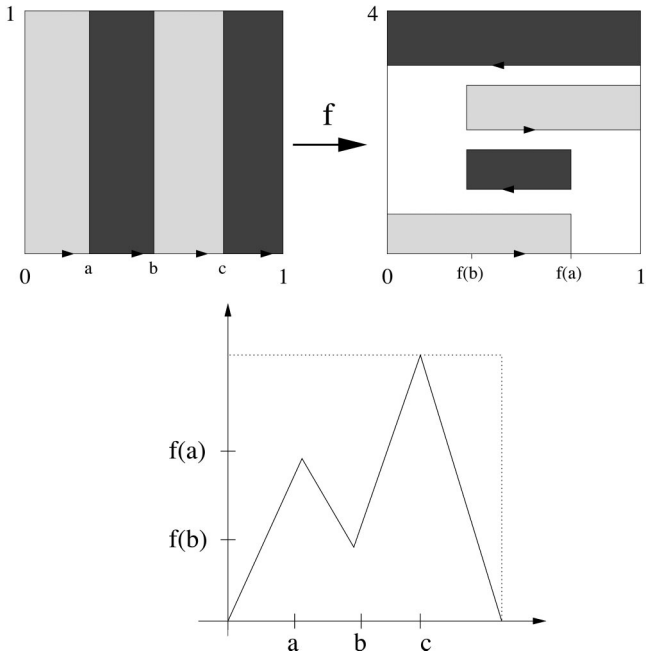

FIG. 12. An extension of a multimodal map. The graph of the factor map is below the extension. Note that the vertical direction in the range of f has been shortened.

the points at which $\eta'(y)=0$ may be dense, depending on the orbit of the critical point of f. However, since we have assumed that (6) holds, the contraction will make the large images of this ''wrinkle'' very small, so that the set will still be approximated well by a smooth manifold. Thus, the only possible self-intersections will only be visible under very high magnification. The closer we are to the bifurcation the larger the magnification necessary to detect these potential loops. However, if $\phi'(x)D_2g(f(x),\phi(x))$ changes sign at x_*, then the left-hand and right-hand limits of $\phi'(f(x))$ are both infinite but disagree in sign, implying a cusp.

In our specific example, $(u,\phi(u))$ maps to $(f(u),c\phi(u)+g(f(u)))$. The function f is increasing and has a critical point at $s=0$, when $u=\rho, v<\alpha$. Thus, the synchronization set has a cusp exactly when it has a minimum (or maximum) at $u=\rho$. For ρ near 1/2, this can be achieved by varying the coupling parameter c.

VI. AN ALTERNATIVE CONSTRUCTION

In Sec. IV A we illustrated the construction of an invariant collection of continuous graphs for system (4), but did not address the smoothness of the graphs in the collection. In this section we show how to introduce an invariant map with an invariant foliation which can be used to address this question directly, and use a similar idea to explain the structure of attractors of the systems introduced in Sec. II B.

As a simple example of the construction once again consider the tent map (2). A map $g:Y\to Y$ is a factor of a map $f:X\to X$ if there exists a map $\phi:X\to Y$ such that $\phi(f(x))=g(\phi(x))$. It is easy to see that the tent map is a factor of the baker's map

$$x_1'=F_1(x_1)=\begin{cases}2x_1 & x_1<1/2\\ -2x_1+1/2 & x_1\geqslant 1/2,\end{cases} \tag{13}$$

$$x_2'=F_2(x_1,x_2)=\begin{cases}\alpha x_2 & x_1<1/2\\ \alpha x_2+(2-\alpha) & x_1\geqslant 1/2,\end{cases} \tag{14}$$

where $\alpha<1$. In this case $\phi:[0,1]\times[0,2]\to[0,1]$ is the projection onto the x axis, so that $\phi(x,y)=x$ is the projection onto the x axis (see Fig. 11). Note that by choosing α close to 1, the amount of contraction in the x_2 direction can be made arbitrarily small.

This map is not invertible on the entire unit square, since the inverse is not defined outside of the shaded areas of Fig. 11. Since we are only interested in the invariant graph over the attractor, we can either extend the map arbitrarily to an invertible map of the plane, or restrict the map to its attractor. The map is discontinuous, but only along the line $x_1=1/2$.

Using a similar construction, we can extend any map $f:[0,1]\to[0,1]$ with finitely many critical points, to an invertible map of a rectangle $[0,1]\times[0,N]$ where N is the number of critical points. An example is given in Fig. 12.

We can therefore associate a system

$$x_{n+1}=F(x_n),\quad y_{n+1}=G(\phi(x_n),y_n), \tag{15}$$

with system (4) where F is invertible. If A is the attractor of (15), then $\tilde{\phi}(A)$ is the attractor of (4), where $\tilde{\phi}$ is the projection to the first and third coordinates $\tilde{\phi}(x_1,x_2,y)=(x_1,y)$.

We can use this extension to discuss the smoothness of the graph over the attractor of the driving map. Since the extended map is invertible, the usual theory of invariant manifolds can be applied away from the orbits of points of discontinuity—corresponding to the orbits of the critical points of the map—which are expected to form a small set. The graph over attractor A of (15) is the restriction of the invariant manifold to this set. Since the projection $\tilde{\phi}$ is smooth, any existing curves in A will be projected smoothly to curves in $\tilde{\phi}(A)$. The contraction in the map can be made arbitrarily small, so that the smoothness of this manifold depends only on the contraction of the noninvertible map used in the construction.

We use a similar argument to explain the structure of the synchronization set observed in Sec. II B, where the Lorenz system was used as a drive. Let f denote the Poincaré map defined on the section $z=27, |x|<8$. There is a stable invariant foliation in the vicinity of the attractor in this Poincaré section.[18] If we denote the projection along this stable foliation by ϕ, the map $\tilde{f}(x)=f(\phi(x))$ is a noninvertible map of the interval which is discontinuous at a single point, and monotone away from this point. If we consider $\tilde{f}$ as the driving map in a drive–response system of type (4), the theory discussed in Sec. III can be applied to construct a tree of intervals and an invariant collection of graphs with a transversal Cantor-type structure. Since the map $\tilde{f}$ if is not uniformly expanding, the arguments about the smoothness of the graphs in the collection require delicate estimates. Since the only critical point of $\tilde{f}$ is the point of discontinuity, the different graphs in the collection will not be connected. A particular projection of this invariant collection of graphs is what is observed in Fig. 2.

We emphasize that in this situation there exists an invariant graph $\Psi:\mathbb{R}^3\to\mathbb{R}$. The attractor of the full four-dimensional system lies in this invariant graph. What is observed in Fig. 2 is a section of the attractor in this invariant graph. Since the dissipation of the Poincaré map in this case is very strong, this section is very thin in the direction of the stable foliation. The section is therefore very close to its projection under ϕ, and hence we observe an object close to one which can be described using the arguments of Sec. III. A similar argument explains the structure of the attractor in the case of the Rössler system, although we are not aware of a proof of the existence of an invariant foliation in this case.

We expect that strongly dissipative systems will result in attractors with similar structures when used as drives in this type of drive–response systems. In such cases the structure in the strongly contracted directions may, in a sense, be resolved in the response system.

VII. CONCLUSION

We have shown that the attractors of certain drive–response systems in general lie on an invariant collection of graphs of functions from the phase space of the driving system to the phase space of the response. Although this collection may have a very complex geometry, under certain conditions it can be approximated by a finite collection of nearly invariant graphs. This explains the occurrence of striated structures frequently observed in in numerical and physical experiments.[7,32]

It is likely that the attractors in many dissipative systems have strong stable foliations along which they can be projected to lower dimensional, noninvertible systems.[18,34] Moreover, noninvertibility is a natural occurrence in many numerical and physical experiments. The arguments given in this paper are applicable in many such cases, and can show that certain response systems could provide an effective way of studying the structure of their attractor.

We have not addressed several interesting questions: It is clear from Fig. 1 that the different graphs in the invariant collection will intersect at various points. Where do these intersections occur? It would also be interesting to estimate a dimension of the attractor as a function of the coupling strength. We end with a discussion of the addition of noise.

In a drive–response system, synchronization sets are global attractors. Therefore, results on random attractors show that additive noise will not change the inherent structure of the attractor but only cause it to spread out.[8] In particular, the attractor is upper semicontinuous, meaning that the Hausdorff semidistance from the noisy attractor to the true attractor approaches zero as the noise intensity limits to zero.

For the both of the systems shown in Fig. 1, we performed numerical experiments comparing the effect of adding noise to the drive to the effect of a noisy response. In the quadratic response case, for a large range of d values ($0.1 \leqslant d \leqslant 0.5$), the noise added to the drive had less of an effect than the same noise added to the response. For the sine response, the effect was reversed for a large range in k ($0.1 \leqslant k \leqslant 0.6$). This difference in relative strengths appears to be the result of the relative dissipation rate determined by the choice of the response. The results of these simulations are available at the URL in Ref. 33.

ACKNOWLEDGMENTS

K.J. was partially supported by Grant No. NSF-0244529. E.S. was partially supported by George Mason University Provost's Office summer research funding.

APPENDIX: Γ_A IS A CONTRACTION

Let Ψ_a and Φ_a be two sequences of graphs in G_a. Then

$$\begin{aligned}
&d_i(\Gamma_{a_i}(\Psi^i_{a_i}),\Gamma_{a_i}(\Phi^i_{a_i}))\\
&\quad=\sup_{x\in J^i_{a_i}}|\Gamma_{a_i}(\Psi^i_{a_i})(x)-\Gamma_{a_i}(\Phi^i_{a_i})|\\
&\quad=\sup_{x\in J^i_{a_i}}|g(f_{a_{i+1}}(x),\Psi^{i+1}_{a_{i+1}}(f^{-1}_{a_{i+1}}(x)))\\
&\qquad-g(f_{a_{i+1}}(x),\Phi^{i+1}_{a_{i+1}}(f^{-1}_{a_{i+1}}(x)))|\\
&\quad<e^{\lambda}\sup_{x\in J^{i+1}_{a_{i+1}}}|\Psi^{i+1}_{a_{i+1}}(x)-\Phi^{i+1}_{a_{i+1}}(x)|\\
&\quad=e^{\lambda}d_{i+1}(\Psi^{i+1}_{a_{i+1}},\Phi^{i+1}_{a_{i+1}}),
\end{aligned}\tag{A1}$$

where the second to last inequality follows from (6).

Inequality (A1) implies directly that

$$\begin{aligned}
\overline{d}_{\eta}(\Gamma_a(\Psi_a),\Gamma_a(\Phi_a))&\leqslant\sum_{i=0}^{\infty}e^{\lambda}\frac{d_{i+1}(\Psi^{i+1}_{a_{i+1}},\Phi^{i+1}_{a_{i+1}})}{e^{\eta i}}\\
&=e^{\lambda+\eta}\sum_{i=0}^{\infty}\frac{d_{i+1}(\Psi^{i+1}_{a_{i+1}},\Phi^{i+1}_{a_{i+1}})}{e^{\eta(i+1)}}\\
&\leqslant e^{\lambda+\eta}\sum_{i=0}^{\infty}\frac{d_i(\Psi^i_{a_i},\Phi^i_{a_i})}{e^{\eta i}}\\
&=e^{\lambda+\eta}\overline{d}_{\eta}(\Psi_a,\Phi_a),
\end{aligned}\tag{A2}$$

and choosing η so that $\lambda + \eta < 0$ ensures that Γ_a is a contraction on G_a. It follows from the contraction mapping theorem that there exists an invariant sequence of graphs $\Psi_a^* \in G_a$.

[1] S. Boccaletti, J. Kurths, G. Osipov, D. L. Valladares, and C. S. Zhou, "The synchronization of chaotic systems," Phys. Rep. **366**, 1–101 (2002).

[2] A. Pikovsky, M. Rosenblum, and J. Kurths, *Synchronization: A Universal Concept in Nonlinear Science* (Cambridge University Press, Cambridge, 2003).

[3] S. Strogatz, *Sync: The Emerging Science of Spontaneous Order* (Hyperion, New York, 2003).

[4] S. Boccaletti, L. Pecora, and A. Pelaez, "Unifying framework for synchronization of coupled dynamical systems," Phys. Rev. E **63**, 066219 (2001).

[5] N. F. Rulkov, M. Suschik, L. S. Tsimring, and H. Abarbanel, "Generalized synchronization of chaos in directionally coupled chaotic systems," Phys. Rev. E **51**, 980–994 (1995).

[6] V. Afraimovich, A. Cordonet, and N. Rulkov, "Generalized synchronization of chaos in noninvertible maps," Phys. Rev. E **66**, 016208 (2002).

[7] E. Barreto, K. Josić, C. J. Morales, E. Sander, and P. So, "The geometry of chaos synchronization," Chaos **13**, 151–164 (2003).

[8] J. C. Robinson, "Stability of random attractors under perturbation and approximation," J. Diff. Eqns. **186**, 652–669 (2002).

[9] P. So, E. Barreto, K. Josić, E. Sander, and S. J. Schiff, "Limits to the experimental detection of nonlinear synchrony," Phys. Rev. E **65**, 046225 (2002).

[10] D. He, Z. Zheng, and L. Stone, "Detecting generalized synchrony: An improved approach," Phys. Rev. E **67**, 026223 (2003).

[11] K. Josić, "Synchronization of chaotic systems and invariant manifolds," Nonlinearity **13**, 1321–1336 (2000).

[12] C. E. Frouzakis, R. A. Adomaitis, I. G. Kevrekidis, M. P. Golden, and B. E. Ydstie, "The structure of basin boundaries in a simple adaptive control system," in *Chaotic Dynamics (Patras, 1991)*, Vol. 298 of NATO Adv. Sci. Inst. Ser. B Phys. (Plenum, New York, 1992), pp. 195–210.

[13] E. N. Lorenz, "Computational chaos—A prelude to computational instability," Physica D **35**, 299–317 (1989).

[14] N. Rulkov and V. Afraimovich, "Detectability of non-differentiable generalized synchrony," Phys. Rev. E **67**, 066218 (2003).

[15] N. Rulkov, V. Afraimovich, L. Lewis, J.-R. Chazottes, and A. Cordonet, "Multivalued mappings in generalized chaos synchronization," Phys. Rev. E **64**, 016217 (2001).

[16] B. R. Hunt, E. Ott, and E. Rosa, "Sporadically fractal basin boundaries of chaotic systems," Phys. Rev. Lett. **82**, 3597–3600 (1999).

[17] J. Guckenheimer and R. F. Williams, "Structural stability of Lorenz attractors," Inst. Hautes Études Sci. Publ. Math. **50**, 59–72 (1979).

[18] W. Tucker, "A rigorous ODE solver and Smale's 14th problem," Found. Comput. Math. **2**, 53–117 (2002).

[19] E. Lorenz, "Deterministic nonperiodic flows," J. Atmos. Sci. **20**, 130–141 (1963).

[20] E. Sander, E. Barreto, K. Josic, and P. So, "Synchronization sets in drive-response systems," in SIAM DSWeb Online Picture Gallery (http://www.dynamicalsystems.org/pi/sm/detail?item=35, 2003).

[21] N. Fenichel, "Persistence and smoothness of invariant manifolds for flows," Indiana Univ. Math. J. **21**, 193–226 (1971/1972).

[22] M. W. Hirsch, C. C. Pugh, and M. Shub, *Invariant Manifolds*, Lecture Notes in Mathematics, Vol. 583 (Springer, Berlin, 1977).

[23] J. Stark, "Regularity of invariant graphs for forced systems," Ergod. Theory Dyn. Syst. **19**, 155–199 (1999).

[24] S. B. Nadler, Jr., *Continuum Theory, An Introduction*, Vol. 158 of Monographs and Textbooks in Pure and Applied Mathematics (Dekker, New York, 1992).

[25] M. Barge and W. T. Ingram, "Inverse limits on [0, 1] using logistic bonding maps," Topology Appl. **72**, 159–172 (1996).

[26] V. Afraimovich, J.-R. Chazottes, and A. Cordonet, "Synchronization in directionally coupled systems: Some rigorous results," Discrete Contin. Dyn. Syst. B **1**, 421–442 (2001).

[27] M. Barge, K. Brucks, and B. Diamond, "Self-similarity in inverse limit spaces of the tent family," Proc. Am. Math. Soc. **124**, 3563–3570 (1996).

[28] P. Minc and W. R. R. Transue, "A transitive map on [0, 1] whose inverse limit is the pseudoarc," Proc. Am. Math. Soc. **111**, 1165–1170 (1991).

[29] D. Hadjiloucas, M. J. Nicol, and C. P. Walkden, "Regularity of invariant graphs over hyperbolic systems," Ergod. Theory Dyn. Syst. **22**, 469–482 (2002).

[30] W. S. Mahavier, "Arcs in inverse limits on [0, 1] with only one bonding map," Proc. Am. Math. Soc. **21**, 587–590 (1969).

[31] G. W. Henderson, "The pseudo-arc as an inverse limit with one binding map," Duke Math. J. **31**, 421–425 (1964).

[32] J. Chubb, E. Barreto, P. So, and B. Gluckman, "The breakdown of synchronization in systems of nonidentical chaotic oscillators: Theory and experiment," Int. J. Bifurcation Chaos Appl. Sci. Eng. **11**, 2705–2713 (2001).

[33] K. Josic and E. Sander, "Noisy synchronization sets for noninvertible drives" (http://math.gmu.edu/~sander/research/josicsander/).

[34] R. F. Williams, "One-dimensional non-wandering sets," Topology **6**, 473–487 (1967).